Author Manuscript

Author Manuscript

Author Manuscript

Author Manuscript

HHS Public Access

Author manuscript

*J Orthop Res*. Author manuscript; available in PMC 2021 January 01.

Published in final edited form as:

*J Orthop Res*. 2020 January ; 38(1): 105–116. doi:10.1002/jor.24395.

# Amplifying bone marrow progenitors expressing alpha smooth muscle actin produce zonal insertion sites during tendon-to-bone repair

**Timur B. Kamalitdinov**[1], **Keitaro Fujino**[1,2], **Snehal S. Shetye**[1], **Xi Jiang**[1], **Yaping Ye**[1], **Ashley B. Rodriguez**[1], **Andrew F. Kuntz**[1], **Miltiadis H. Zgonis**[1], **Nathaniel A. Dyment**[1]

[1]McKay Orthopaedic Research Laboratory, Department of Orthopaedic Surgery, University of Pennsylvania, Philadelphia, PA, USA

[2]Department of Orthopedic Surgery, Osaka Medical College, Osaka, Japan

## Abstract

Traditional tendon-to-bone repair where the tendon is reattached to bone via suture anchors often results in disorganized scar production rather than the formation of a zonal insertion. In contrast, ligament reconstructions where tendon grafts are passed through bone tunnels can yield zonal tendon-to-bone attachments between the graft and adjacent bone. Therefore, ligament reconstructions can be used to study mechanisms that regulate zonal tendon-to-bone repair in the adult. Anterior cruciate ligament (ACL) reconstructions are one of the most common reconstruction procedures and while we know that cells from outside the graft produce the attachments, we have not yet established specific cell populations that give rise to this tissue. To address this knowledge gap, we performed ACL reconstructions in lineage tracing mice where alpha smooth muscle actin (αSMACreERT2) was used to label αSMA-expressing progenitors within the bone marrow that produced zonal attachments. Expression of αSMA was increased during early stages of the repair process such that the contribution of SMA-labeled cells to the tunnel integration was highest when tamoxifen was delivered in the first week post-surgery. The zonal attachments shared features with normal entheses, including tidemarks oriented perpendicularly to collagen fibers, Col1a1-expressing cells, alkaline phosphatase activity, and proteoglycan-rich staining. Finally, the integration strength increased with time, requiring 112% greater force to remove the graft from the tunnel at 28 compared to 14 days post-surgery. Future studies will target these progenitor cells to define the pathways that regulate zonal tendon-to-bone repair in the adult.

Corresponding author: Nathaniel A. Dyment, Ph.D., Assistant Professor of Orthopaedic Surgery and Bioengineering, McKay Orthopaedic Research Laboratory, Department of Orthopaedic Surgery, University of Pennsylvania, 330A Stemmler Hall, 3450 Hamilton Walk, Philadelphia, PA 19104-6081, Fax: 215-573-2133, dyment@pennmedicine.upenn.edu.

Author contributions:

Experiment conception and design completed by TBK, KF, SSS, XJ, AFK, MHZ, NAD. Experiment execution completed by TBK, KF, SSS, XJ, YY, ABR. Data analysis and interpretation completed by TBK, KF, SSS, XJ, YY, ABR, AFK, MHZ, NAD. The paper was written and edited by TBK, KF, SSS, XJ, YY, ABR, AFK, MHZ, NAD. All authors approve the submitted manuscript.

Author Manuscript Author Manuscript Author Manuscript Author Manuscript

**Keywords**

tendon-to-bone repair; ACL reconstruction; alpha smooth muscle actin; mineralized cryohistology; transgenic mice

## INTRODUCTION

Tendon and ligament injuries affect approximately 30% of adults in the United States[1], with many tendon injuries occurring near the bony attachment site, or enthesis. Surgical repair represents one treatment option to improve function and decrease pain. Despite extensive research aimed at improving surgical outcomes, repair failure remains a common problem[2–8]. High failure rates may be due to a tendon environment that does not support a prompt, effective healing response[9]. Moreover, healing following tendon-to-bone repair results in disorganized scar formation rather than re-establishment of zonal tendon-to-bone attachments. In contrast, when a tendon is placed through a bone tunnel, zonal attachments with collagen fibers spanning across unmineralized and mineralized fibrocartilage occur[10–18]. While direct tendon repairs typically are not performed through a bone tunnel (due to anatomic constraints), ligament reconstructions often utilize a tendon graft placed though bone tunnels. The anterior cruciate ligament (ACL) is one of the most common reconstructed ligaments. In this study, a mouse model of ACL reconstruction, similar to a previous work[19–21], is used. Because of the vast array of transgenic mouse models, specific cell populations can be genetically modified to better understand the mechanisms of the repair process. There is a critical need to establish the key regulators that lead to zonal tendon-to-bone attachments in such a model, in order to translate these findings to novel tendon-to-bone repair therapies in which repair through a bone tunnel cannot be performed.

A staged repair response ensues after tendon grafts are passed through bone marrow tunnels in the femur and tibia following ACL reconstruction that ultimately leads to zonal tendon-to-bone attachments at the interface of the tendon graft and adjacent bone marrow[10–18,22]. The cellular origin of these attachments is not from tenocytes within the tendon graft but instead from external populations as demonstrated by studies using GFP allografts or physical barriers around the tendon graft[11,23,24]. As these studies were performed in large animals with limited genetic models, specific identification of the cellular origin could not be elucidated. Since these attachments occur at the interface between the tendon graft and the adjacent bone marrow, presumably mesenchymal progenitors within the bone marrow give rise to cells that repopulate the tendon graft and form zonal attachments.

There are several murine genetic models used previously to identify resident mesenchymal stem/progenitor cells that give rise to new bone, cartilage, and tendon tissue following injury[25–30]. One such Cre model is driven by the promoter for the alpha smooth muscle actin (αSMA) gene (Acta2). This model labels a resident multipotent progenitor within the bone marrow that gives rise to new bone and adipocytes during growth and development. It also labels quiescent progenitor populations in the periosteum[25,26], paratenon[27,31], skeletal muscle[32], and dental pulp[33] that activate in response to injury. Additionally, αSMA is highly expressed by these cell populations during the early proliferative phase of the repair

Author Manuscript Author Manuscript Author Manuscript Author Manuscript

response. Therefore, αSMA could be a potential marker of progenitors within the bone marrow that may participate in the tunnel integration process following ACL reconstruction.

In the current study, we utilized transgenic lineage tracing and real time fluorescent reporter mice to measure the contribution of bone marrow progenitors to zonal tendon-to-bone attachments following ACL reconstruction. The ability of these cells to produce zonal attachments in the tunnels was assessed using multiplexed mineralized cryohistology where we can clearly delineate between mineralized fibrocartilage of zonal attachments vs. adjacent newly formed trabecular bone. The objective of this study was to measure the contribution of cells expressing αSMA at different stages of the repair process to fibrochondrocytes within zonal tendon-to-bone attachments and osteocytes within adjacent bone following ACL reconstruction. Our hypothesis was that quiescent mesenchymal progenitor cells within the bone marrow were primary contributors to tendon-to-bone attachments within bone tunnels following ACL reconstruction. Since αSMA is expressed by amplifying bone marrow progenitors, targeting the cells during this phase will also label a higher proportion of cells that contribute to the tendon-to-bone attachments and adjacent bone.

## METHODS

### Mice

All animal procedures were approved by the University of Pennsylvania's institutional animal care committee. The transgenic mouse lines used in this study were described previously: αSMACreERT2[25,26], R26R-tdTomato Cre reporter (B6;129S6-Gt(ROSA)26Sortm9(CAG-tdTomato)Hze/J, stock # 007905)[34], and Col1a1(3.6kb)-CFP fluorescent reporter mice (STOCK Tg(Col1a1*3.6-Cyan)2Rowe/J, stock # 017468)[25,35–37]. The three lines were crossed together to yield triple and double (Cre-negative) transgenic mice. Cre recombination was induced by intraperitoneal injection (80 mg/kg) of tamoxifen (Sigma-Aldrich Corp.). Demeclocycline (60 mg/kg) injections were given the day prior to sacrifice to label deposited mineral, specifically the tidemark within zonal attachments.

### Experimental design

ACL reconstructions (ACLR) were performed on a total of 61 mice (mean ± SD age, 16.0 ± 1.6 weeks old) while uninjured controls were also included (total = 65 mice) (Fig. 1). Three tamoxifen injections groups were included: i) $T_{-14}$ group received tamoxifen injections on 14, 11, and 8 days prior to surgery, ii) $T_0$ group received tamoxifen injections on the day of surgery, 3, and 6 days post-surgery, and iii) $T_7$ group received tamoxifen injections on 7, 10, and 13 days post-surgery. Mice were assigned to either histological or biomechanical assessment. Histology mice were assigned to the day after the last injection: uninjured control for $T_{-14}$ group (n = 4), 7 days post-surgery for $T_0$ group (n = 6), and 14 days post-surgery for the $T_7$ group (n = 8). Additional mice were harvested at 28 days post-surgery for $T_{-14}$ (n = 5), $T_0$ (n = 6), and $T_7$ (n = 9) injection groups. Additional mice that were double transgenic (Cre-negative) were assigned for immunostaining on days 7, 14, and 28 (n = 2 per group). Two biomechanical assays were performed: anterior drawer and tunnel pullout tests. Anterior drawer tests were performed on mice right after surgery (n = 8) and

Author Manuscript Author Manuscript Author Manuscript Author Manuscript

compared to contralateral uninjured limbs. Tunnel pullout tests were performed on mice at 14 (n = 7) and 28 (n = 6) days post-surgery. Both male and female sexes were included and were equally distributed across the treatment groups.

### ACL reconstruction procedure using tail tendon autografts

The right knee joint of each mouse was subjected to surgical transection of the ACL followed by reconstruction (Fig. 2 and S1). Mice were anesthetized with isoflurane (1% −3%), given pre-surgical analgesia, and sterilely prepped. An anteromedial incision was made adjacent to the patellar tendon and the patella was subluxed laterally to access the joint space (Fig. 2A1). The ACL was transected with a 27G needle. After confirmation of substantially increased anterior drawer and intact PCL, a 27G needle was used to hand drill the tibial tunnel originating as close to the native ACL footprint as possible and exiting on the medial cortex of the tibia within the metaphysis (Fig. 2A2). Then, a new 27G needle was used to drill the femoral tunnel originating at the native ACL footprint and exiting on the lateral surface of the femur proximal to the patella (Fig. 2A3). Next 7–8 tail tendons (length = 3–4 cm) were harvested (Fig. S1D) from the same mouse as a bundle (mean diameter of bundle = 490 μm) and maintained in PBS to prevent dehydration. A 27G needle was inserted antegrade into the tibial tunnel and suture was wrapped around the mid-length of the tail tendon bundle and passed through the needle (Fig. S1E). Once the suture, but not the tail tendons, were through the needle, the needle was removed and the tendon graft was pulled through the tunnel from the suture (Fig. S1F). A similar procedure was performed to pass the tendon graft through the femoral tunnel (Fig. S1G–H). Once the mid-length of the tendon graft was outside the femoral tunnel, it was passed through and around a 316 stainless steel washer (OD 1.98 mm, ID 1.0 mm; McMaster Carr) to anchor the graft to the washer (i.e., cow hitch knot) at the outer cortex of the femur (Fig. S1J–K). The knee was positioned near full extension and then the two ends of the tail tendon graft at the outside of the tibia were tied to another stainless steel washer using a surgical knot such that the washer was positioned as closely to the outer cortex as possible (Fig. S1L). The patella was then placed back to its anatomical position and the patellar tendon and medial retinaculum were sutured closed followed by skin closure. After recovery from anesthesia, the animals were returned to their cage and allowed to move ad libitum. At assigned time points, mice were euthanized via $CO_2$ asphyxiation.

### Anterior drawer test

Following euthanasia, left hindlimbs were isolated and all extraneous soft tissue was removed via sharp dissection. All capsule ligaments, including the cruciates and collaterals, along with the menisci were left intact. The distal half of each tibia was potted in poly(methyl methacrylate) (PMMA). The potted tibial end was fixed in a custom fixture on the material testing machine (Instron 5542, Instron Inc., Norwood, MA) that allowed for adjustment of tibial plateau angle (Fig. 3A). The distal end of the femur was lowered into another custom fixture that allowed for control of knee flexion by rotating the femur around the joint center of rotation. The knee joint was tested for anterior and posterior stability by cyclic loading between ±0.4N at 0.1N/sec for 10 cycles and the 10th cycle was used to quantify maximum anterior and posterior displacements. Samples are defined as: Intact – intact left knee, ACLT – ACL transected left knee (transected on testing machine after

Author Manuscript Author Manuscript Author Manuscript Author Manuscript

testing intact), ACLR – ACL reconstructed right knee, ACLRT – ACLR graft transected right knee (transected on testing machine after testing ACLR).

### Multiplexed mineralized cryohistology

Following euthanasia, hindlimbs were harvested and fixed in formalin for 2 days, transferred to 30% sucrose overnight, and embedded in OCT. Tape-stabilized, frozen mineralized sagittal sections[35,38,39] of the knee were collected and each section was subjected to three rounds of imaging on the Zeiss Axio Scan.Z1 digital slide scanner including 1) fluorescent reporters, mineralization label, and polarized light, 2) alkaline phosphatase (AP) fluorescent staining (Vector Blue Alkaline Phosphatase Substrate Kit, Vector Laboratories) with Hoechst 33342 counterstain, and 3) 0.025% toluidine blue (TB) or hematoxylin and eosin (aqueous) staining. Sections were decalcified prior to alkaline phosphatase staining. The sections displayed in figure 5 were stained with toluidine blue, imaged, then the stain was removed with Immunocal (Statlab), stained for H&E, and finally imaged again such that 4 rounds of imaging occurred. Layered composite images of all imaging rounds were assembled and aligned in image editing software.

Additional Cre-negative double transgenic mice were stained with a mouse anti-αSMA Cy3-conjugated antibody (Millipore Sigma, clone 1A4, 1:200) and an anti-endomucin antibody (Santa Cruz, V.7C7, 1:50) with goat anti-rat Alexa Fluor 647-conjugated secondary antibody (ThermoFisher Scientific, 1:200).

### Tunnel pullout test

Following euthanasia, mice were frozen until the day of testing. Limbs were dissected similar to the anterior drawer test and the femur and tibia were potted in PMMA. The knee was disarticulated and the femur was mounted on the testing machine such that the tunnel was aligned parallel to the linear actuator. A 2–0 suture was passed through the washer on the outer cortex of the femur and loaded uniaxially (0.025mm/sec) until failure. The same procedure was repeated for the tibial tunnel. Maximum loads were recorded for pullout strength.

### Image analysis

The contribution of SMA-labeled cells to the tunnel integration was assessed at 28 days post-surgery for each injection group ($T_{-14}$, $T_0$, and $T_7$) by quantifying the number of tdTomato+ cells within the mineralized fibrocartilage of the tunnel attachments and the osteocytes in the surrounding trabecular bone. The mineralized fibrocartilage was identified by highly aligned collagen fibers (polarized light filter) traversing through a fluorescent tidemark (i.e., demeclocycline). Trabecular bone within 500 μm of the tunnel edge was included in the osteocyte measurements. The cells were identified by segmenting the cell nuclei and then corresponding 8-bit values within the tdTomato channel were recorded. An equivalent minimum threshold was applied to each image to determine the percentage of cells that were tdTomato+. The percentage of Col1-CFP+ cells and the percent area of alkaline phosphatase staining were also measured within the unmineralized fibrocartilage of the tunnel attachments. The region of interest was defined by regions of attachments where

Author Manuscript Author Manuscript Author Manuscript Author Manuscript

the tidemark was perpendicular to the collagen fibers and extended 200 μm from the tidemark towards the graft midsubstance.

### Statistics

All data were normally distributed. The anterior and posterior drawer results were compared between groups (intact, ACLT, ACLR, and ACLRT) via one-way ANOVA with Bonferroni post-hoc comparisons ($p < 0.05$). The number of Col1-CFP+ cells and the percent area of AP staining within the unmineralized fibrocartilage of the attachments were compared across time points via one-way ANOVAs ($p < 0.05$). The contribution of SMA-labeled cells to mineralized fibrocartilage and adjacent bone at day 28 were compared between the different injection groups ($T_{-14}$, $T_0$, and $T_7$) via one-way MANOVA with Tamhane post hoc comparisons for unequal variance ($p < 0.05$). The pullout strengths at days 14 and 28 post-surgery were compared via one-tailed t-test with unequal variance ($p < 0.05$).

## RESULTS

### The ACL reconstruction procedure restored 45% of anterior stability of knee

Intact knees experienced 0.11±0.06 mm of anterior displacement at 0.4 N (Fig. 3C). Following transection of the ACL on the testing machine such that the starting position was consistent between intact and ACLT knees, the anterior displacement increased to 1.03±0.15 mm ($p < 0.05$). ACLR knees experienced 0.68±0.20 mm of anterior displacement at 0.4N and increased to 1.10±0.23 mm following transection of the tendon graft on the testing machine ($p < 0.05$). We conducted the test in this fashion because we were concerned that we would not be able to find the neutral zone of the knee joint when loading the ACLR knee onto the testing machine. However, we found that both left and right knees, when tested in their ACL-deficient state, displayed similar levels of anterior displacement ($p > 0.05$). Nonetheless, we also calculated the difference in maximum anterior displacement for the knee prior to (i.e., intact or ACLR) and after transection (i.e., ACLT or ACLRT). The difference in anterior displacement at 0.4N was 0.92±0.11 mm between intact and ACLT groups and 0.42±0.21 mm for ACLR and ACLRT groups. Therefore, the ACL reconstruction procedure restored 45% of anterior stability of the knee.

The ACL reconstruction procedure did have an effect on the posterior stability of the knee as the surgery often caused partial damage to the posterior cruciate ligament (PCL) (Fig. 3D). Therefore, intact (−0.16±0.07mm) and ACLT (−0.20±0.07 mm) knees displayed significantly less drawer in the posterior direction than both the ACLR (−0.50±0.21 mm) and ACLRT (−0.51±0.21 mm) knees ($p < 0.05$). However, the posterior drawer did not change between intact and ACLT groups, indicating that the PCL was not damaged when the ACL was transected on the testing machine.

### Zonal tendon-to-bone attachments develop through a coordinated spatiotemporal process

Following the bone tunnel injury in the ACL reconstruction procedure, bone marrow mesenchymal progenitor cells activated within the first week post-surgery and began to infiltrate the periphery of the tail tendon graft (Fig. 4A1–3) to initiate tendon-to-bone attachments while the resident cells of the tail tendon graft slowly died over time, leading to

Author Manuscript Author Manuscript Author Manuscript Author Manuscript

acellular regions of the graft (Figs. 4A and 5A). The infiltrating cells expressed Col1-CFP as they initiated the attachment (Fig. 4D). These cells also expressed alkaline phosphatase at the day 7 time point. However, there was no demeclocycline within the attachments, indicating mineral had not been deposited. On the other hand, disorganized woven bone with Col1-CFP+ and AP+ osteoblasts formed along the tunnel periphery (Fig. 4A).

By 14 days post-surgery (Fig. 4B), cells within the attachment produced mineralized fibrocartilage resulting in organized tidemarks (via demeclocycline) oriented perpendicular to the collagen fibers (Fig. 4B3), similar to a native enthesis[35]. In these attachments, Col1-CFP+ and AP+ cells were situated within the unmineralized zone with AP being more concentrated near the tidemark (Fig. 4B2). The adjacent trabecular bone became more organized by 14 days post-surgery with less woven bone. By 28 days post-surgery, the attachments continued to mature (Fig. 4C). The number of Col1-CFP+ cells and the AP activity within the unmineralized regions of the attachments remained consistent over these time points (Fig. 4D, $p < 0.05$).

The zonal attachments, while more disorganized, shared common characteristics with native entheses (Fig. 5A). These characteristics included proteoglycan-rich unmineralized and mineralized zones of fibrocartilage consisting of collagen fibers traversed by a tidemark (Fig. 5A2, tidemark denoted by yellow line). The multiplexed cryohistology used in this study, which combines undecalcified sectioning with multiple rounds of fluorescent and chromogenic imaging, assisted in identifying the zonal attachments compared to standard histological stains. Polarized light microscopy was used to visualize the collagen fibers in combination with demeclocycline imaging to identify tidemarks running perpendicular to the collagen fibers in order to identify the zonal attachment (Fig. 5A2) vs adjacent mineralizing bone (Fig. 5A3). In addition, toluidine blue staining was used to identify proteoglycan-rich regions of these attachments (Fig. 5), which is indicative of fibrocartilage. The strength of the demeclocycline tidemark and Col1-CFP expression were also increased in the zonal attachments (Fig. 5A2) compared to native adult entheses (Fig. 5A1 and S2B), suggesting higher mineral deposition rates and collagen transcription.

## αSMA is transiently expressed in the activated bone marrow and early tendon-to-bone attachments

In order to visualize the spatiotemporal expression patterns of endogenous αSMA in the repair tissues, samples were stained with an anti-αSMA-Cy3 antibody at days 7, 14, and 28 post-surgery. αSMA staining was concentrated within vascular (i.e., smooth muscle cells) and perivascular regions of the contralateral uninjured limbs (yellow arrows in Fig. S3A). Within the repair tissue, αSMA staining was concentrated in the bone marrow adjacent to the tunnels that responded to the injury (“AM” in Fig. S3B1–2). These regions of the marrow displayed stronger eosin staining compared to peripheral and uninjured marrow (“M” in Fig. S3B2 and S3A2, respectively). αSMA staining was also found in cells infiltrating the graft at day 7 (“A” in Fig. S3B1) but staining diminished in these regions as the attachments mineralized by day 14 (“A” in Fig. S3C1). The level of staining in the marrow adjacent to the tunnel diminished from day 7 to day 14 (Fig. S3B2 vs. S3C2) and was near baseline levels at day 28 (data not shown). Finally, a subset of cells in the adjacent

Author Manuscript Author Manuscript Author Manuscript Author Manuscript

marrow and early attachments co-expressed αSMA and Col1-CFP (green arrows in Fig. S3) while others were Col1-CFP negative, with a subset of negative cells being adjacent to vessels within the bone marrow (Fig. S4C).

### αSMA-expressing bone marrow progenitor cells contribute to the tunnel integration

Since αSMA is expressed by bone marrow mesenchymal progenitor cells[25], we utilized αSMACreERT2 in combination with the Ai9 R26R-tdTomato Cre reporter to label these cells via tamoxifen injections at 14, 11, and 8 days prior to surgery ($T_{-14}$ group in Fig. 6A). In an uninjured limb on the day after the last injection, tdTomato expression was found in several cell populations including those within the primary spongiosa (Fig. 6A1), periosteum (Fig. 6A2), and near the surface of trabecular bone (Fig. 6A3). In addition, a small subset of cells were tdTomato+ within the patellar tendon midsubstance and epitenon. Strong labeling was also found within perivascular cells and smooth muscle cells throughout the bone marrow, joint space, and muscle. Finally, we also analyzed tail tendons from these mice and found that while there was stronger labeling in the epitenon, only 0.74±0.68% of cells within the tail tendon midsubstance were tdTomato+ (Fig. S5).

When mice in the $T_{-14}$ injection group received ACL reconstructions and then were analyzed at 28 days post-surgery, there were tdTomato+ cells within the tail tendon graft, unmineralized and mineralized regions of the attachments, and within the surrounding trabecular bone (Fig. 7A, D, E). The contribution of SMA-labeled cells was similar within the mineralized fibrocartilage of the attachments (4.0±4.7%, Fig. 7D) vs. osteocytes in the surrounding trabecular bone (2.9±1.6%, Fig. 7E) ($p > 0.05$).

### Increased αSMA expression during early stages of repair resulted in the $T_0$ injection group having the highest cellular contribution to zonal attachments and adjacent bone

Since αSMA is induced in response to injury in a variety of mesenchymal tissues including tendon, periosteum, and bone marrow[25–27,31] (Fig. S3), we studied two additional injection groups defined as $T_0$ (injections on 0, 3, and 6 days post-surgery) and $T_7$ (injections on 7, 10, and 13 days post-surgery). We found a higher percentage of tdTomato+ cells within mineralized fibrocartilage (MFC) as well as the surrounding trabecular bone in the $T_0$ group compared to the $T_{-14}$ injection group ($p < 0.05$, Fig. 7D–E), with the $T_7$ group displaying an increasing trend in the MFC ($p = 0.08$) compared to $T_{-14}$. The $T_0$ group also had a higher percentage of tdTomato+ cells in both the MFC and bone than the $T_7$ group ($p < 0.05$, Fig. 7D–E).

### Pullout strength of the femoral tunnel increased with healing time

To directly test the extent of tunnel integration, we conducted tunnel pullout tests for tibial and femoral tunnels separately (Fig. 8). Therefore, the knee was disarticulated prior to loading the femur and tibia in separate grips. The knot around the stainless steel washer on the tibia was not strong enough to resist loads experienced during the test, resulting in the knot failing before the graft was pulled out of the tunnel. As a result, the tibial tunnel tests were not included in our analysis. The femoral washer was anchored sufficiently to the tendon graft with the cow hitch knot and there was no evidence of slipping at the washer

Author Manuscript Author Manuscript Author Manuscript Author Manuscript

during the test. The pullout strength of the femoral tunnel was greater at day 28 (1.06±0.27 N) compared to day 14 (0.50±0.25 N) post-surgery ($p < 0.05$, Fig. 8B).

## DISCUSSION

Constructing the spatiotemporal events needed to create a zonal tendon-to-bone insertion site are critical to producing a functional repair outcome. Traditional tendon-to-bone repair where the tendon is reattached to bone with suture leads to scar formation instead of a zonal enthesis. As seen in this study (Figs. 4, 5, and 7), ligament reconstructions where a tendon is passed through a bone tunnel, such as the femoral and tibial tunnels in an ACL reconstruction procedure, can yield zonal attachments of the tendon graft to the adjacent bone[10–18]. Therefore, ligament reconstructions can be used to study the mechanisms of zonal tendon-to-bone repair. While it is well appreciated that cells from outside the tendon graft contribute to the tunnel integration process[11,22–24], the specific cell populations that give rise to zonal attachments and newly formed bone during this process are poorly understood.

To this end, we utilized the αSMACreERT2 model to specifically target cells participating in the repair at multiple time points before ($T_{-14}$) and after ($T_0$ and $T_7$) surgery. This mouse model was previously shown to target an amplifying osteoprogenitor population within the growing metaphysis[25]. In addition, it labels quiescent adult progenitors within periosteum[25,26], epitenon[27,31], skeletal muscle[32], and dental pulp[33] that activate in response to injury. Unlike growing bone, fewer quiescent mesenchymal progenitors within the adult bone marrow express αSMA compared to the periosteum, therefore there is minimal contribution of these cells to intramembranous bone formation within the medullary cavity following injury[40]. We found similar results following ACL reconstruction in this study where the contribution of SMA-labeled cells was rather low (Fig. 7A, D, E) when the cells were targeted prior to injury ($T_{-14}$ group) but was significantly improved when tamoxifen was delivered post-surgery (Fig. 7B, D, E) because αSMA is upregulated in the bone marrow that responds to the injury (Fig. S3). Overall, the αSMACreERT2 model is an efficient tool to target bone marrow progenitors that give rise to zonal attachments and newly formed bone adjacent to the bone tunnels (Fig. 7D, E).

Several coordinated stages occur to form the zonal attachments in the bone tunnels, initiating with the expansion of the progenitor pool in the adjacent bone marrow (Figs. 6B2 and S3B). αSMA is expressed by a subset of quiescent progenitors ($T_{-14}$ group) but is also elevated within the amplifying progenitor pool following injury ($T_0$ and $T_7$ groups). These mesenchymal progenitor cells go on to infiltrate the periphery of the tail tendon graft to initiate attachments by day 7 (Figs. 4A, 6B1, and S6A). On day 14 and onward, the cells within these attachments further differentiate and mineralize the surrounding matrix to create zonal attachments consisting of unmineralized and mineralized fibrocartilage zones (“M” in Fig. 5) with collagen fibers spanning across an organized tidemark (Fig. 5A2). While not nearly as organized, the zonal attachments share common features with developing entheses[35] beyond the collagen organization and tidemark stated previously. These attachments contain Col1-CFP+ cells within the unmineralized zones and strong alkaline phosphatase activity concentrated near the tidemark (Fig. 4B–D). In addition,

Author Manuscript Author Manuscript Author Manuscript Author Manuscript

proteoglycan staining (toluidine blue) is found in these attachments (Fig. 5A2). Further investigation is needed to better define the similarities and differences between the process that produces these zonal attachments in adults compared to entheses during normal growth and development. Of particular interest to our lab, future studies will determine whether pathways that regulate zonal enthesis formation during growth and development also have a similar role in zonal tendon-to-bone repair in this surgical model.

In addition to the unmineralized and mineralized fibrocartilage of the attachment, SMA-labeled cells also produce the adjacent trabecular bone to which these attachments are anchored. The question still remains whether the SMA-labeled cells are a heterogeneous mixture of progenitors with a subset primed to form attachments while others are primed to form bone or if a common progenitor exists that gives rise to both tissues. Additional studies in our lab demonstrated that both attachments and adjacent bone come from GDF5-expressing cells (data not shown) that may originate from embryonic stages. Similar to the fate decision that specifies enthesis from tendon midsubstance progenitors in utero[41–43], it will be important to identify an analogous fate decision in this repair model and the pathway(s) that regulate such a decision. With the availability of an array of inducible Cre mouse lines labeling a variety of cell types including osteoprogenitors[28–30] and tenogenic cells[44], such an analysis can now be conducted. In fracture healing, αSMA-expressing periosteal progenitors give rise to both chondrocytes and osteocytes in the fracture callus[25,26]. When these periosteal progenitors from an early callus were isolated and cultured in vitro, they were capable of multipotent differentiation[26], suggesting that it is possible a common progenitor could give rise to both zonal attachments and adjacent bone following ACL reconstruction. Determining whether a common cell population needs to be driven down two separate differentiation paths (zonal attachment vs. bone) or two distinct cell populations need to be present to form these separate tissues could provide key guidance for successful tendon-to-bone repair strategies. Future investigation of these mechanisms is needed and is a focus of our work moving forward.

In addition to the transient expression by a subset of quiescent and amplifying progenitors in mesenchymal tissues[25–27,31,32,37,45], αSMA is also a common marker of myofibroblasts[46–48]. The convenience of a unique molecular marker for these cells have led to a common misconception that mesenchymal cells that expresses αSMA must be myofibroblasts[46,49]. However, the key defining features of myofibroblasts are the *de novo* development of *in vivo* stress fibers and contractile forces[46,49]. Fibroblasts transiently differentiate into αSMA-negative protomyofibroblasts before differentiating further into αSMA-positive myofibroblasts[47,49]. There is minimal evidence indicating that myofibroblasts are progenitors or are multipotent, which suggests that the SMA-labeled cells that produce the zonal attachment and/or adjacent bone did not arise from a myofibroblast population. However, this point does not negate the possibility that certain tdTomato+ cells in this study were myofibroblasts. Future studies will work to further identify sub-populations of SMA-labeled cells that are progenitors giving rise to zonal attachments and/or bone vs. local myofibroblasts.

This study is not without limitations. First, we were unable to fully restore the anterior stability of the knee following the reconstruction procedure. This was primarily because the

Author Manuscript Author Manuscript Author Manuscript Author Manuscript

tunnels could not be drilled perfectly on the native footprints of the ACL without fracturing the epiphyses, particularly in the tibia. Second, we were unable to produce perfectly aligned longitudinal sections along the graft in the tibial tunnel, joint space, and femoral tunnel. This is in part because the femoral and tibial tunnels were drilled independently of each other so it is nearly impossible to align both tunnels during fixation. To address this limitation, we first aligned the block to produce longitudinal sections within the femoral tunnel, then adjusted the block to attempt to align the tibial tunnel, resulting in poor alignment of the graft within the joint space. Finally, the tail tendon knot tied around the washer at the exit of the tibial tunnel failed during the tunnel pullout test. We are modifying our protocol to stably grip this tissue to address this limitation in future studies.

Identifying the key mechanisms that regulate zonal tendon-to-bone repair requires that we have model systems that yield zonal repairs and can be spatiotemporally controlled such that modulation of specific factors can improve or impair these attachments. By doing so, we can define specific genes or pathways that positively or negatively regulate the process. Findings in these studies will guide future therapies to target these mechanisms to improve the repair outcome. With the vast genetic tools available with transgenic mouse lines, the ACL reconstruction model in this study and the αSMACreERT2 mouse can serve as a test platform to specifically target cells, genes, and pathways that regulate zonal tendon-to-bone repair. Future studies will focus on key signaling pathways that have been shown to regulate zonal enthesis formation during growth and development.

## Supplementary Material

Refer to Web version on PubMed Central for supplementary material.

## ACKNOWLEDGEMENTS

This study was funded by NIH R00 AR067283, the Penn Center for Musculoskeletal Disorders (P30 AR069619), the Penn Thomas B. McCabe and Jeannette E. Laws McCabe Fund, and startup funds from the Orthopaedic Surgery Department at the University of Pennsylvania.

## REFERENCES

1. Praemer A, Furner S, Rice DP. 1999 Musculoskeletal Conditions in the United States. American Academy of Orthopaedic Surgeons, Rosemont, IL p. 182.
2. Galatz LM, Sandell LJ, Rothermich SY, et al. 2006 Characteristics of the rat supraspinatus tendon during tendon-to-bone healing after acute injury. J Orthop Res 24(3):541–550. [PubMed: 16456829]
3. Patel S, Caldwell J-M, Doty SB, et al. 2018 Integrating soft and hard tissues via interface tissue engineering. J Orthop Res 149(4):89–1077.
4. Dyment NA, Galloway JL. 2015 Regenerative Biology of Tendon: Mechanisms for Renewal and Repair. Curr Mol Bio Rep 1(3):124–131. [PubMed: 26389023]
5. Derwin K, Amini M, Ricchetti E, Iannotti J. 2015 Rotator cuff repair: challenges and solutions. Orthop Res Rev 7:57–69.
6. Nourissat G, Berenbaum F, Duprez D. 2015 Tendon injury: from biology to tendon repair. Nat Rev Rheumatol 11(4):223–233. [PubMed: 25734975]
7. Thomopoulos S, Parks WC, Rifkin DB, Derwin KA. 2015 Mechanisms of tendon injury and repair. J Orthop Res 33(6):832–839. [PubMed: 25641114]
8. Lu HH, Thomopoulos S. 2013 Functional Attachment of Soft Tissues to Bone: Development, Healing, and Tissue Engineering. Annu Rev Biomed Eng 15(1):201–226. [PubMed: 23642244]

Author Manuscript Author Manuscript Author Manuscript Author Manuscript


9. Edelstein L, Thomas SJ, Soslowsky LJ. 2011 Rotator cuff tears: what have we learned from animal models? J Musculoskelet Neuronal Interact 11(2):150–162. [PubMed: 21625052]
10. Deehan DJ, Cawston TE. 2005 The biology of integration of the anterior cruciate ligament. J Bone Joint Surg 87(7):889–895.
11. Kobayashi M, Watanabe N, Oshima Y, et al. 2017 The Fate of Host and Graft Cells in Early Healing of Bone Tunnel after Tendon Graft. Am J Sports Med 33(12):1892–1897.
12. Rodeo SA, Arnoczky SP, Torzilli PA, et al. 1993 Tendon-healing in a bone tunnel. A biomechanical and histological study in the dog. J Bone Joint Surg 75(12):1795. [PubMed: 8258550]
13. Bedi A, Kawamura S, Ying L, Rodeo SA. 2009 Differences in Tendon Graft Healing Between the Intra-articular and Extra-articular Ends of a Bone Tunnel. HSS Jrnl 5(1):51–57.
14. Carbone A, Carballo C, Ma R, et al. 2016 Indian hedgehog signaling and the role of graft tension in tendon-to-bone healing: Evaluation in a rat ACL reconstruction model. J Orthop Res 34(4):641–649. [PubMed: 26447744]
15. Rodeo SA, Kawamura S, Kim H-J, et al. 2017 Tendon Healing in a Bone Tunnel Differs at the Tunnel Entrance versus the Tunnel Exit. Am J Sports Med 34(11):1790–1800.
16. Hexter AT, Thangarajah T, Blunn G, Haddad FS. 2018 Biological augmentation of graft healing in anterior cruciate ligament reconstruction. Bone Joint J 100-B(3):271–284. [PubMed: 29589505]
17. Tomita F, Yasuda K, Mikami S, et al. 2001 Comparisons of intraosseous graft healing between the doubled flexor tendon graft and the bone–Patellar tendon–Bone graft in anterior cruciate ligament reconstruction. Arthroscopy 17(5):461–476. [PubMed: 11337712]
18. Weiler A, Hoffmann RFG, Bail HJ, et al. 2002 Tendon healing in a bone tunnel. Part II. Arthroscopy 18(2):124–135. [PubMed: 11830805]
19. Camp CL, Lebaschi A, Cong G-T, et al. 2017 Timing of Postoperative Mechanical Loading Affects Healing Following Anterior Cruciate Ligament Reconstruction: Analysis in a Murine Model. J Bone Joint Surg Am 99(16):1382–1391. [PubMed: 28816898]
20. Lebaschi A, Deng XH, Coleman NW, et al. 2017 Restriction of Postoperative Joint Loading in a Murine Model of Anterior Cruciate Ligament Reconstruction: Botulinum Toxin Paralysis and External Fixation. J Knee Surg 30(7):687–693. [PubMed: 27907934]
21. Deng XH, Lebaschi A, Camp CL, et al. 2018 Expression of Signaling Molecules Involved in Embryonic Development of the Insertion Site Is Inadequate for Reformation of the Native Enthesis: Evaluation in a Novel Murine ACL Reconstruction Model. J Bone Joint Surg 100(15):e102. [PubMed: 30063598]
22. Ekdahl M, Wang JH-C, Ronga M, Fu FH. 2008 Graft healing in anterior cruciate ligament reconstruction. Knee Surg Sports Traumatol Art 16(10):935–947.
23. Kleiner JB, Amiel D, Roux RD, Akeson WH. 2005 Origin of Replacement Cells for the Anterior Cruciate Ligament Autograft. J Orthop Res 4(4):1–9.
24. Bachy M, Sherifi I, Zadegan F, et al. 2016 Allograft integration in a rabbit transgenic model for anterior cruciate ligament reconstruction. Orthop Traumatol Surg Res 102(2):189–195. [PubMed: 26775085]
25. Grcevic D, Pejda S, Matthews BG, et al. 2012 In Vivo Fate Mapping Identifies Mesenchymal Progenitor Cells. Stem Cells 30(2):187–196. [PubMed: 22083974]
26. Matthews BG, Grcevic D, Wang L, et al. 2014 Analysis of αSMA-Labeled Progenitor Cell Commitment Identifies Notch Signaling as an Important Pathway in Fracture Healing. J Bone Miner Res 29(5):1283–1294. [PubMed: 24190076]
27. Dyment NA, Hagiwara Y, Matthews BG, et al. 2014 Lineage Tracing of Resident Tendon Progenitor Cells during Growth and Natural Healing. PLoS ONE 9(4):e96113–12. [PubMed: 24759953]
28. Worthley DL, Churchill M, Compton JT, et al. 2015 Gremlin 1 identifies a skeletal stem cell with bone, cartilage, and reticular stromal potential. Cell 160(1–2):269–284. [PubMed: 25594183]
29. Maes C, Kobayashi T, Selig MK, et al. 2010 Osteoblast Precursors, but Not Mature Osteoblasts, Move into Developing and Fractured Bones along with Invading Blood Vessels. Dev Cell 19(2): 329–344. [PubMed: 20708594]

Author Manuscript Author Manuscript Author Manuscript Author Manuscript


30. Kawanami A, Matsushita T, Chan YY, Murakami S. 2009 Mice expressing GFP and CreER in osteochondro progenitor cells in the periosteum. Biochem Biophys Res Commun 386(3):477–482. [PubMed: 19538944]
31. Yoshida R, Alaee F, Dyrna F, et al. 2016 Murine supraspinatus tendon injury model to identify the cellular origins of rotator cuff healing. Connect Tissue Res 57(6):507–515. [PubMed: 27184388]
32. Matthews BG, Torreggiani E, Roeder E, et al. 2016 Osteogenic potential of alpha smooth muscle actin expressing muscle resident progenitor cells. Bone 84:69–77. [PubMed: 26721734]
33. Vidovic-Zdrilic I, Vining KH, Vijaykumar A, et al. 2018 FGF2 Enhances Odontoblast Differentiation by αSMA+ Progenitors In Vivo. J Dental Res 97(10):1170–1177.
34. Madisen L, Zwingman TA, Sunkin SM, et al. 2009 A robust and high-throughput Cre reporting and characterization system for the whole mouse brain. Nat Neurosci 13(1):133–140. [PubMed: 20023653]
35. Dyment NA, Breidenbach AP, Schwartz AG, et al. 2015 Gdf5 progenitors give rise to fibrocartilage cells that mineralize via hedgehog signaling to form the zonal enthesis. Dev Biol 405(1):96–107. [PubMed: 26141957]
36. Hagiwara Y, Dyment NA, Jiang X, et al. 2015 Fixation stability dictates the differentiation pathway of periosteal progenitor cells in fracture repair. J Orthop Res 33(7):948–956. [PubMed: 25639792]
37. Kalajzic Z, Li H, Wang L-P, et al. 2008 Use of an alpha-smooth muscle actin GFP reporter to identify an osteoprogenitor population. Bone 43(3):501–510. [PubMed: 18571490]
38. Dyment NA, Jiang X, Chen L, et al. 2016 High-Throughput, Multi-Image Cryohistology of Mineralized Tissues. J Vis Exp (115):e54468–e54468.
39. Dyment NA, Hagiwara Y, Jiang X, et al. 2015 Response of knee fibrocartilage to joint destabilization. Osteoarthritis Cartilage 23(6):1–11. [PubMed: 25219671]
40. Matic I, Matthews BG, Wang X, et al. 2016 Quiescent Bone Lining Cells Are a Major Source of Osteoblasts During Adulthood. Stem Cells 34(12):2930–2942. [PubMed: 27507737]
41. Blitz E, Sharir A, Akiyama H, Zelzer E. 2013 Tendon-bone attachment unit is formed modularly by a distinct pool of Scx- and Sox9-positive progenitors. Development 140(13):2680–2690. [PubMed: 23720048]
42. Sugimoto Y, Takimoto A, Akiyama H, et al. 2013 Scx+/Sox9+ progenitors contribute to the establishment of the junction between cartilage and tendon/ligament. Development 140(11):2280–2288. [PubMed: 23615282]
43. Schwartz AG, Long F, Thomopoulos S. 2014 Enthesis fibrocartilage cells originate from a population of Hedgehog-responsive cells modulated by the loading environment. Development 142(1):196–206.
44. Howell K, Chien C, Bell R, et al. 2017 Novel model of tendon regeneration reveals distinct cell mechanisms underlying regenerative and fibrotic tendon healing. Sci Rep 7(45238):1–14. [PubMed: 28127051]
45. Roguljic H, Matthews BG, Yang W, et al. 2013 In vivo Identification of Periodontal Progenitor Cells. J Dent Res 92(8):709–715. [PubMed: 23735585]
46. Hinz B, Phan SH, Thannickal VJ, et al. 2012 Recent Developments in Myofibroblast Biology: Paradigms for Connective Tissue Remodeling. Am J Pathol 180(4):1340–1355. [PubMed: 22387320]
47. Hinz B, Phan SH, Thannickal VJ, et al. 2007 The Myofibroblast: One Function, Multiple Origins. Am J Pathol 170(6):1807–1816. [PubMed: 17525249]
48. Van De Water L, Varney S, Tomasek JJ. 2013 Mechanoregulation of the Myofibroblast in Wound Contraction, Scarring, and Fibrosis: Opportunities for New Therapeutic Intervention. Adv Wound Care 2(4):122–141.
49. Tomasek JJ, Gabbiani G, Hinz B, et al. 2002 Myofibroblasts and mechano-regulation of connective tissue remodeling. Nat Rev Mol Cell Biol 3(5):349–363. [PubMed: 11988769]

Author Manuscript Author Manuscript Author Manuscript Author Manuscript

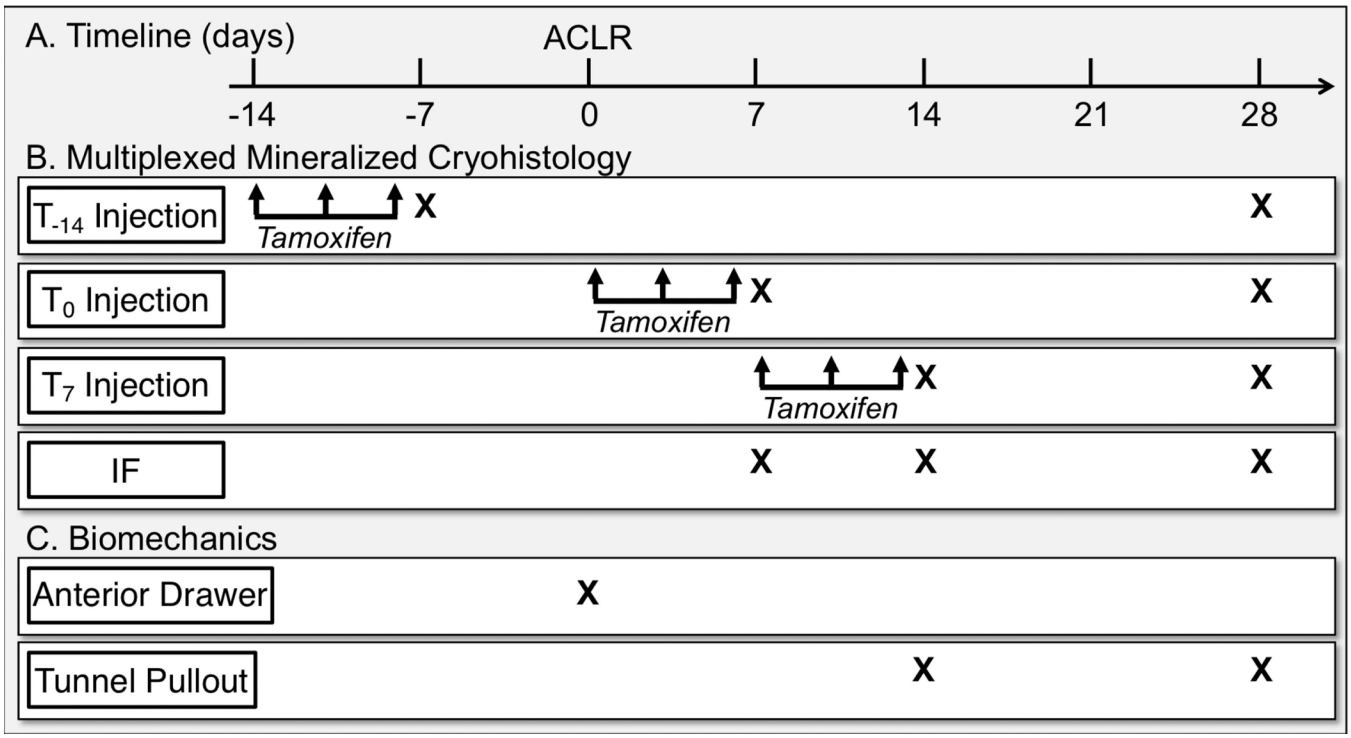


**Fig. 1: Experimental Design.**

αSMACreERT2;R26R-tdTomato;Col1-CFP triple transgenic mice were given three tamoxifen injections starting on either 14 days before surgery ($T_{-14}$), the day of surgery ($T_0$), or 7 days after surgery ($T_7$). Additional Cre-negative mice were assigned for immunofluorescence (IF). Mice were analyzed via multiplexed mineralized cryohistology (B) on defined days (X denotes day of analysis). Additional samples were assigned to either anterior drawer tests just after surgery or tunnel pullout tests at 14 and 28 days post-surgery (C).

Author Manuscript Author Manuscript Author Manuscript Author Manuscript

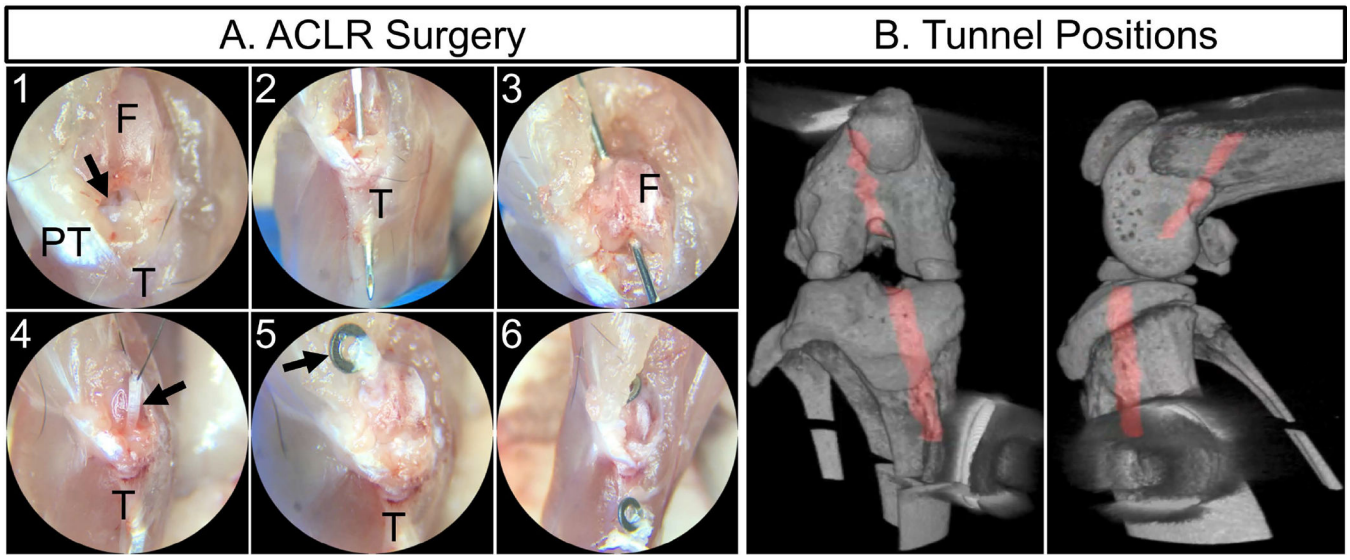


**Fig. 2: ACL reconstruction procedure.**

The ACL (arrow in A1) was accessed with an anteromedial incision and excised near the femoral insertion. The tibial tunnel (2) and femoral (3) tunnels were drilled with 27G needles. The tail tendon graft (arrow in A4) was passed through the tibial tunnel (4) then tied to a stainless steel washer (arrow in 5) after passing through the femoral tunnel. Finally, the graft was tied to another washer outside the tibial tunnel (6) resulting in tunnel positions (red in panel B) as seen via MicroCT.

Author Manuscript
Author Manuscript
Author Manuscript
Author Manuscript



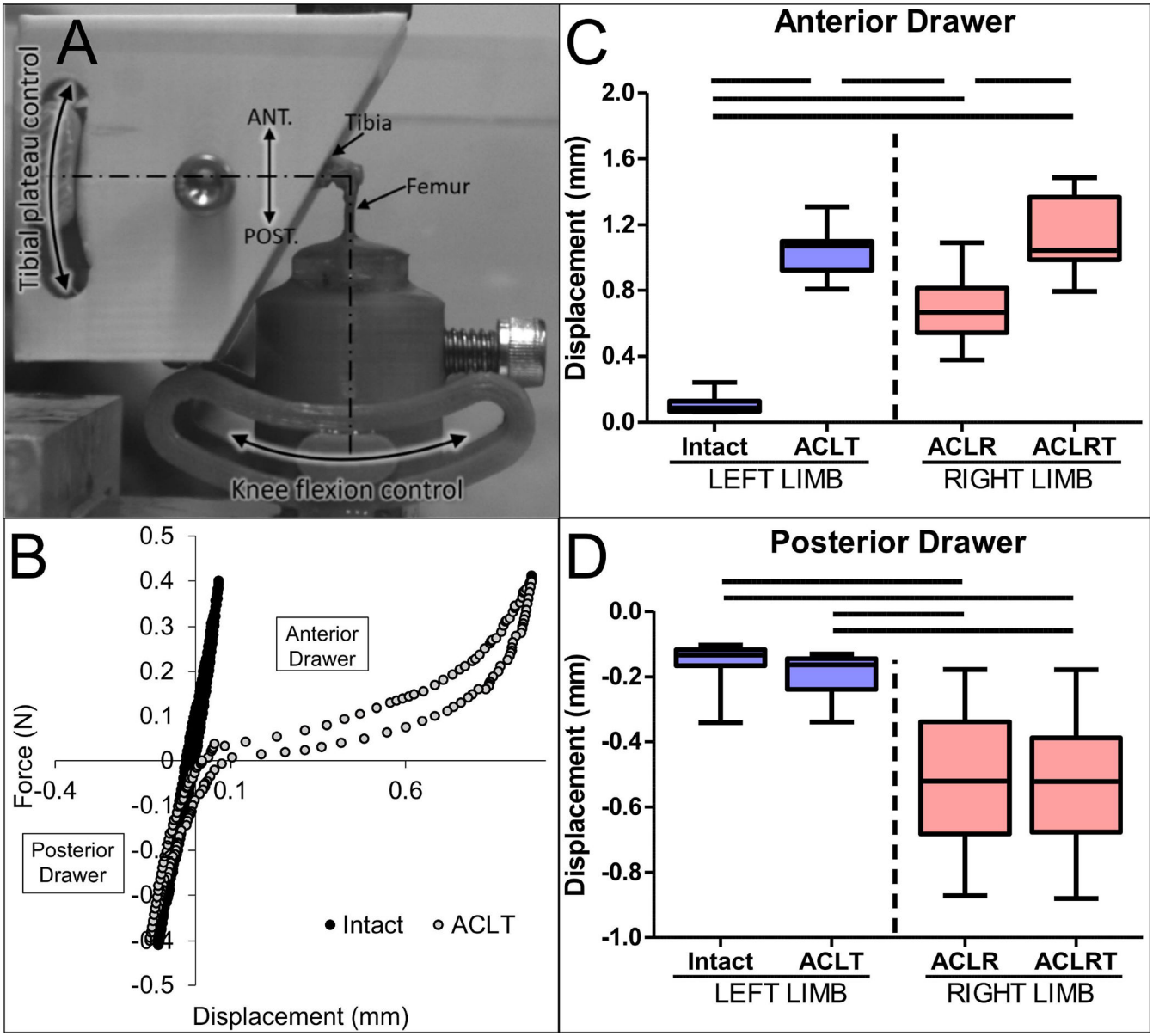


**Fig. 3: ACL reconstruction procedure restored 45% of anterior stability of the knee.**

The tibia and femur were loaded in custom grips that allowed for control of flexion angle (A). Intact and ACLT (transected ACL) states were conducted on left limbs where the ACL was transected on the machine after testing the intact state (B). The same tests were performed on ACLR and ACLRT (transected graft in ACLR knee) states in the right knee. Maximum anterior (C) and posterior (D) displacements for each group were recorded. Bars denote $p < 0.05$ ($n = 8$ per group).

Author Manuscript
Author Manuscript
Author Manuscript
Author Manuscript



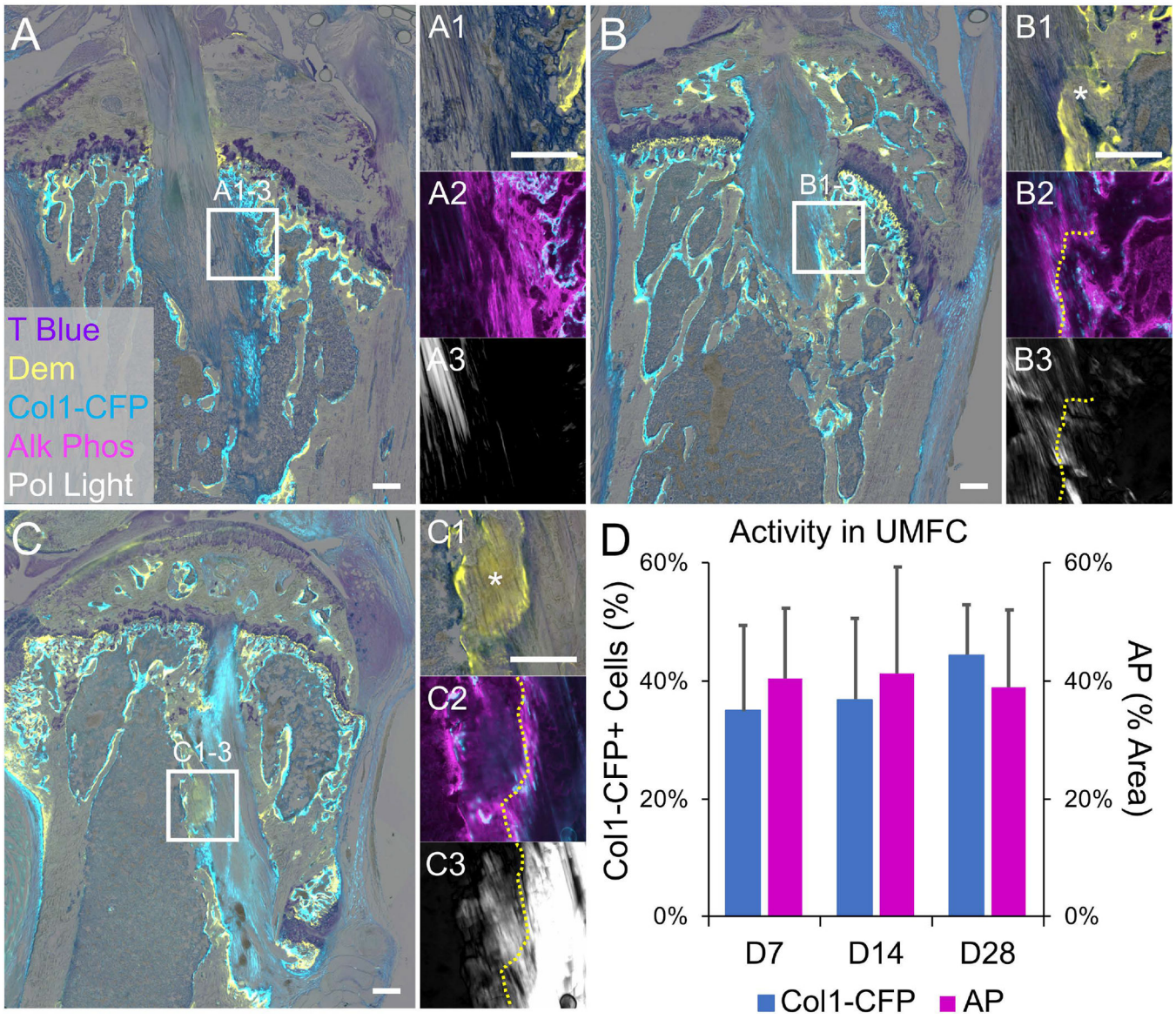


**Fig. 4: Establishment of zonal tendon-to-bone attachments with active collagen expression and mineralization.**

Mineralized frozen sections were made at 7 (A), 14 (B), and 28 (C) days post-surgery and imaged for Col1-CFP reporter (cyan in A, B, C, A2, B2, and C2), demeclocycline (Dem) (yellow in A1, B1, and C1), collagen structure (A3, B3, C3) during the first round of imaging. The section was then stained and imaged for alkaline phosphatase (magenta in A2, B2, and C2) followed by toluidine blue (A, B, C, A1, B1, and C1). Cells infiltrated collagen fibers of the tail tendon at day 7 (A) but mineralization had not occurred. A noticeable tidemark (yellow dotted lines in B and C) was seen in the attachments at 14 and 28 days with mineralized fibrocartilage (* in B1 and C1). Col1-CFP+ cells and alkaline phosphatase activity were located within the unmineralized zones (UMFC) of the attachments (A2, B2, C2) and did not change with time (D, $p > 0.05$) ($n = 4$, 4, and 6 for D7, D14, and D28 groups, respectively). Scale bars = 200μm.

Author Manuscript
Author Manuscript
Author Manuscript
Author Manuscript



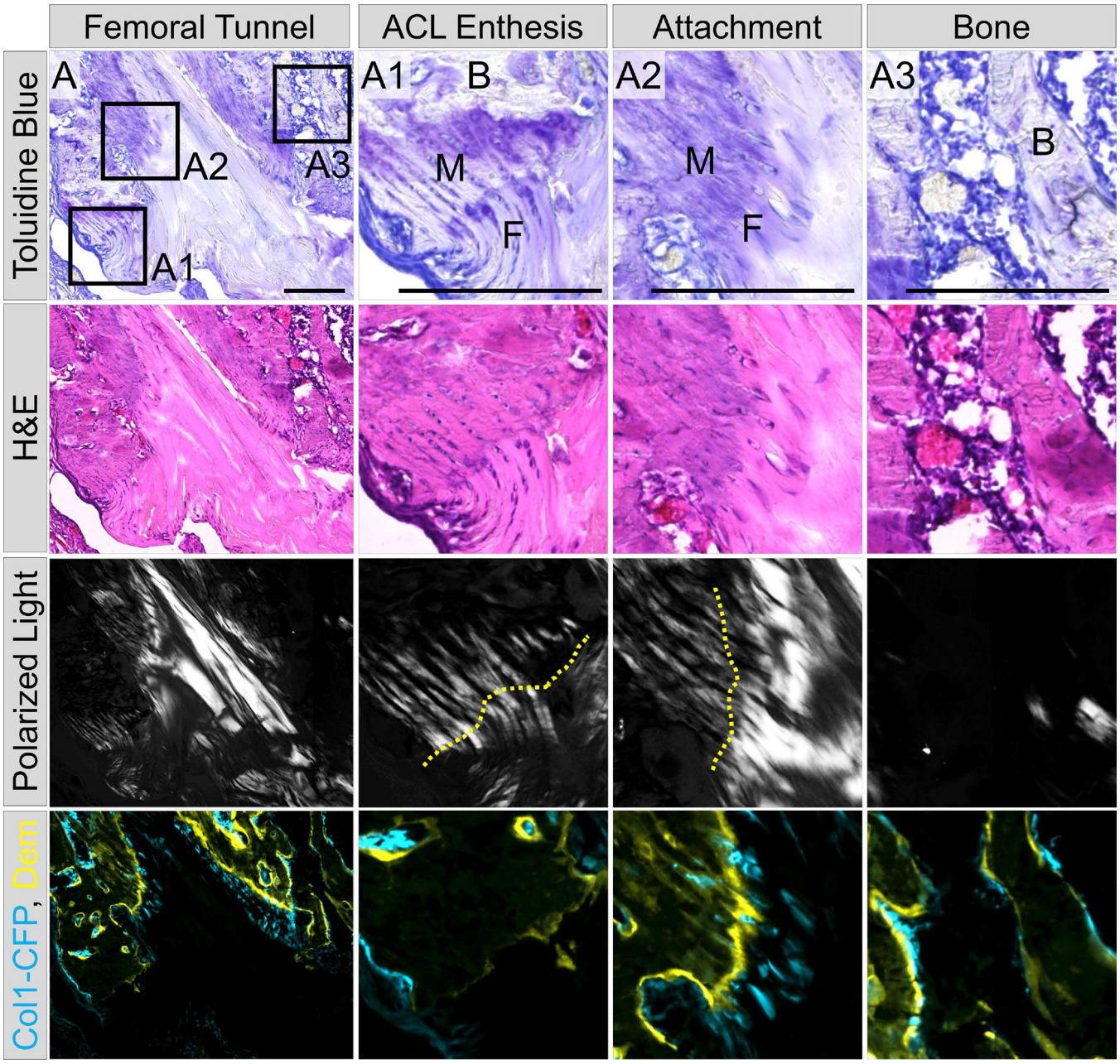


**Fig. 5: Zonal tendon-to-bone attachments share characteristics with native entheses.**

We used several fluorescent and histological criteria to define the zonal attachments. These attachments share features with native entheses more so than the adjacent bone. To highlight these characteristics, this figure includes the remnant of the transected ACL with the femoral enthesis (A1), zonal attachment near the entrance to the femoral tunnel (A2), and adjacent trabecular bone (A3). All panels came from the same section that was imaged 4 times. The first row is toluidine blue which demonstrates strong proteoglycan staining (purple) within the unmineralized (F) and mineralized (M) fibrocartilage of the ACL enthesis and zonal attachment compared to weak staining in the adjacent bone. The second row is H&E staining which highlights the cell morphology within these tissues as well as the established

Author Manuscript Author Manuscript Author Manuscript Author Manuscript

tidemark in the ACL enthesis and zonal attachment. The third row is polarized light imaging which was used to visualize the collagen fibers extending through the unmineralized and mineralized fibrocartilage of the enthesis (A1) and zonal attachment (A2) compared to weak polarized light in adjacent bone (B in panels A1 and A3). Finally, row 4 is a composite image of Col1-CFP (cyan) expression and demeclocycline (Dem, yellow) mineralization labeling demonstrating the expression of Col1a1 within these tissues and the mineral deposition at the tidemarks (A1–2) and bone surface (A3). Scale bars = 200μm. Comparison to the uninjured ACL enthesis can be found in Fig. S2.

Author Manuscript Author Manuscript Author Manuscript Author Manuscript

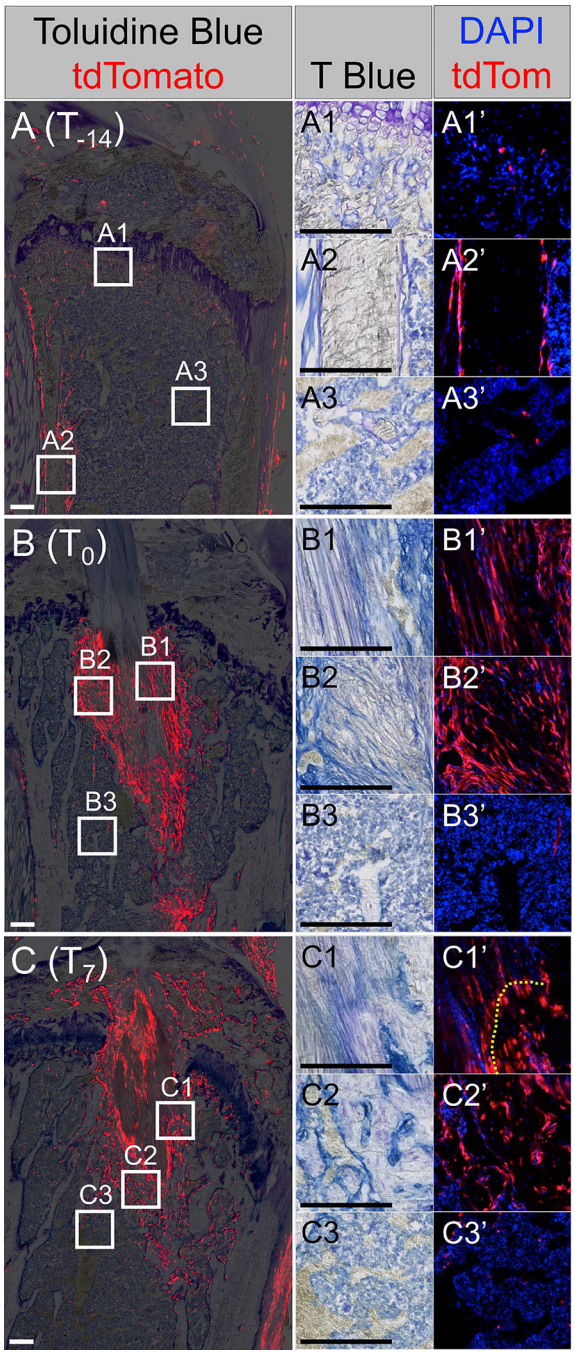


**Fig. 6: αSMACreERT2 line efficiently targets amplifying progenitor population that contributes to tunnel integration.**

Mice in the $T_{-14}$ (A), $T_0$ (B), and $T_7$ (C) groups were assessed on the day after the last injection to determine the cell populations that were labeled. tdTomato+ cells (red) within the primary spongiosa (A1'), periosteum (A2'), and bone marrow (A3') were found in the $T_{-14}$ group. tdTomato+ cells within the attachments (B1' and C1'), adjacent bone (B2' and C2') but not peripheral bone marrow (B3' and C3') were found in the $T_0$ and $T_7$ groups. Insets are either toluidine blue (A1 – C3) or tdTomato (red) with nuclear counterstain (blue)

(A1’ – C3’). Panels B and C are from the same samples as Fig. 4A and 4B, respectively. Scale bars = 200μm.

Author Manuscript Author Manuscript Author Manuscript Author Manuscript

Author Manuscript Author Manuscript Author Manuscript Author Manuscript

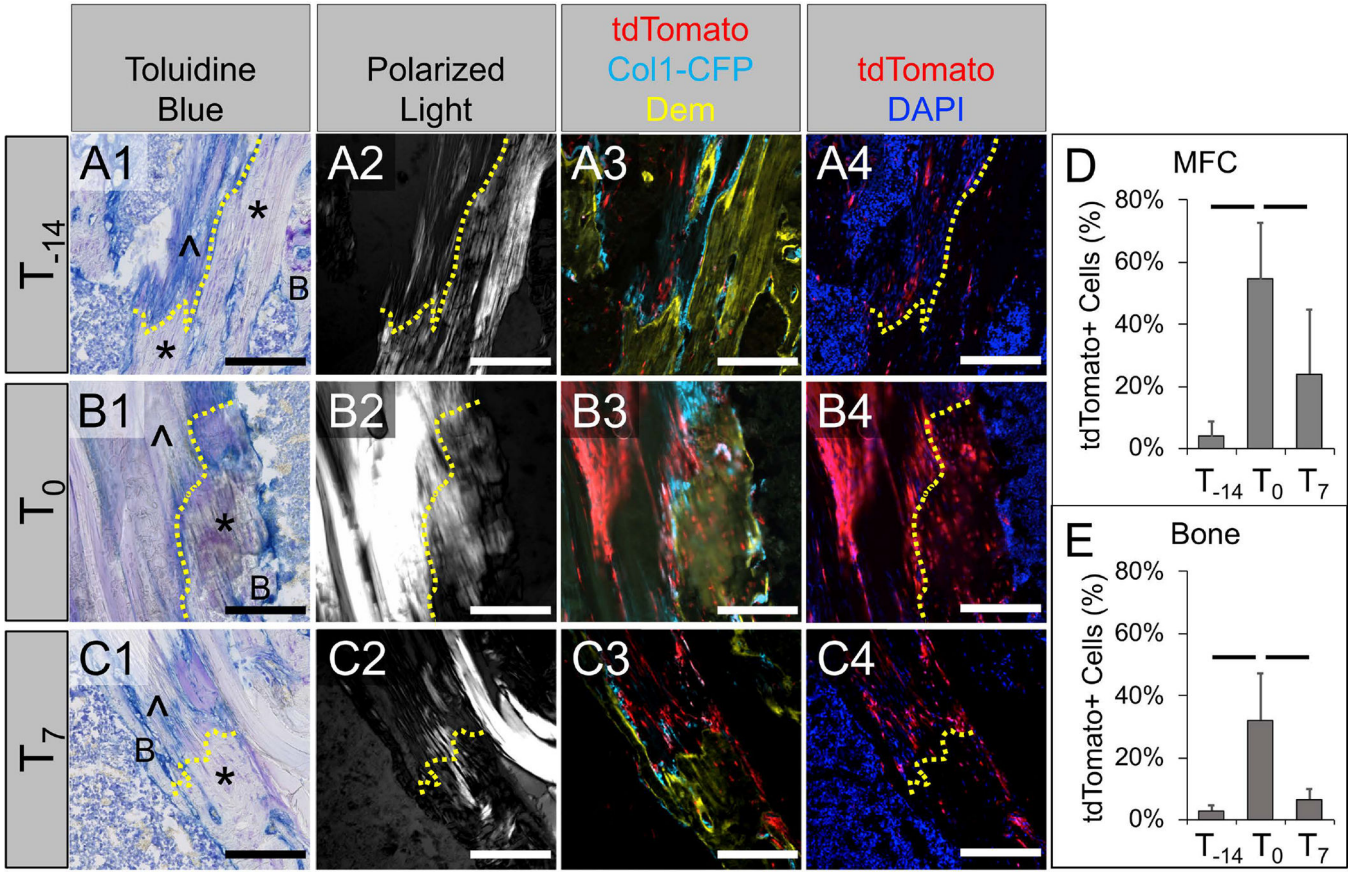


**Fig. 7: The $T_0$ injection group yielded the highest number of SMA-labeled cells within the attachments and adjacent bone.**

Mice from $T_{-14}$ (A), $T_0$ (B), and $T_7$ (C) groups were assessed at 28 days post-surgery to determine the relative contributions of SMA-labeled cells to zonal attachments (D) and adjacent bone (E). Column 1 is toluidine blue, column 2 is collagen structure (polarized microscopy), column 3 is tdTomato (red) and Col1-CFP (cyan) cells with demeclocycline labeling (dem, yellow), column 4 is tdTomato with nuclear counterstain (blue). Dotted lines indicate tidemark location; * indicates mineralized fibrocartilage; ^ indicates unmineralized fibrocartilage; B indicates bone. Images were rotated such that the orientation of each attachment is consistent. Bars in plots denote $p < 0.05$ ($n = 5, 6, 8$ for $T_{-14}$, $T_0$, and $T_7$ groups, respectively). Scale bars = 200μm.

Author Manuscript Author Manuscript Author Manuscript Author Manuscript

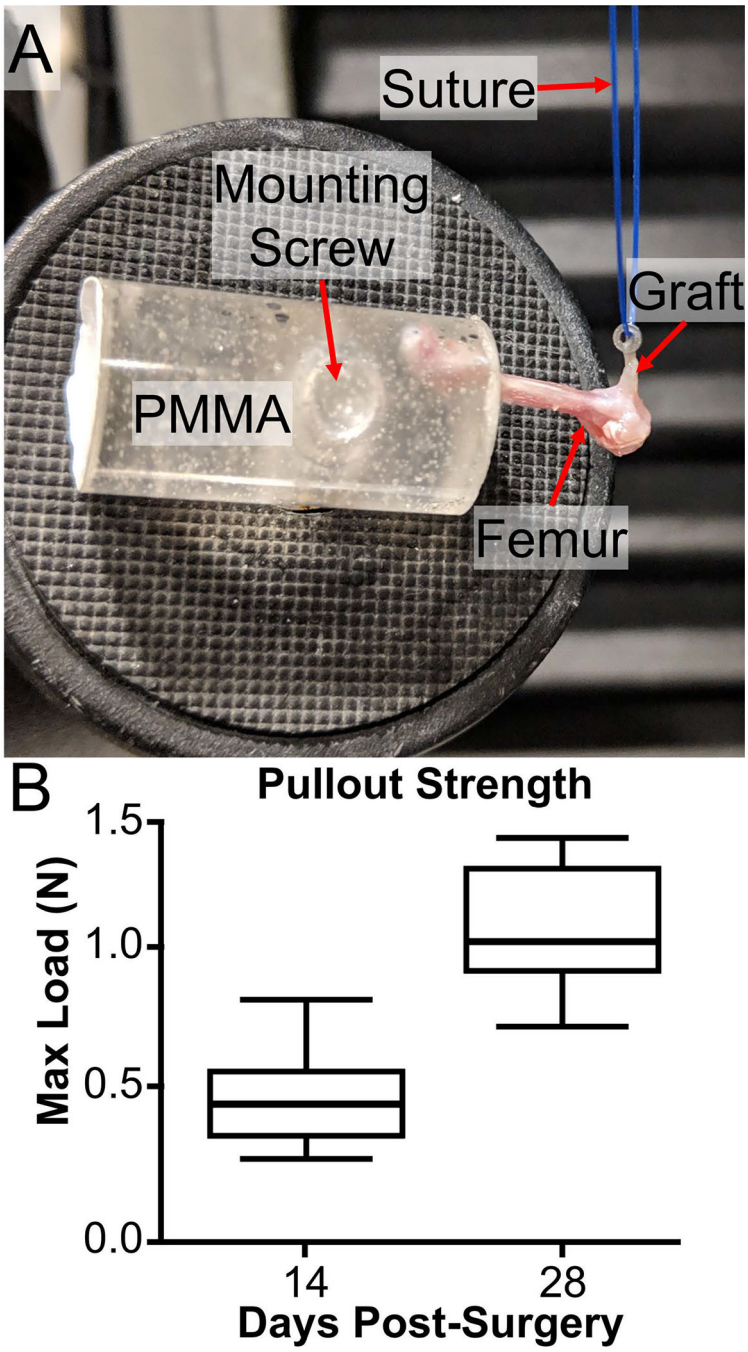


**Fig. 8: Day 28 grafts demonstrated significantly greater pullout strength compared to day 14.**
Femurs were mounted in PMMA while a suture was attached to the washer on the femur as well as the actuator of the testing machine (A). The washer was pulled until the graft was removed from the tunnel as seen in panel A. The maximum loads were recorded and compared between the groups (B) with day 28 being significantly greater than day 14 ($p < 0.05$) ($n = 6–7$ per group).